The Automatic Numerical Processing of Interferometric Transonic Flow Measurements

M. Wehner
EPF Lausanne, Switzerland

P. Bryanston-Cross, T.R. Judge, C. Chenggen
Warwick University, UK

Abstract:

Laser Holographic Interferometry (LHI) at the EPFL (Ecole Polytechnique Fédérale de Lausanne) has been developed over a number of years to provide a direct optical transonic flow diagnostic tool.

It is often convenient, due to the needs of passage instrumentation and blade fixtures, to restrict optical access to one side of the test facility.

To overcome this limitation a reflective holographic system has been devised, which uses one of the internal tunnel walls as a mirror surface. However, due to the movement of the facility spurious vibration information is added to the movement of the transonic flow data.

A numerical method has been developed by Warwick University and demonstrated on the Laval nozzle flow facility at EPFL which uses an FFT (Fast Fourier Transform) algorithm to remove the superimposed background information. It then uses a method known as phase unwrapping to extract numerical quantitative data from the interferometrically formed images automatically.

An example is presented of the transonic flow around an aerofoil section within the Laval nozzle.

* Ecole Polytechnique Fédérale de Lausanne, Laboratoire de Thermique appliquée et de Turbomachines (LTT), Switzerland

** Optical Engineering Group, Warwick University, United Kingdom

1 INTRODUCTION

Quantitative optical diagnostics have now been developed such that it is possible to obtain an instantaneous non-intrusive description of a transonic flow-field.

In the work presented in this paper laser holographic interferometry (LHI) has been used to achieve such a visualisation. The test described was the result of a long history of such optical measurements; beginning with the development of an optical system for application to a 2D turbine cascade described in ref. (1) & (2) and more recently in the automatic numerical extraction of data from a 2D aerofoil section. Ref. (3).

Conventionally LHI has required a clear line of sight through the wind tunnel, to allow the light beam to pass through the flow field of interest. This allows a measurement to be of the density field which in turn can then be used to calculate the velocity and static pressure distributions within the flow. In many of the cases of interest, a clear optical line of sight across the flow is not possible, due either to blade fixturing or instrumentation. In these situations a reflection based optical system is seen as advantageous.

A reflecting holographic system has been designed by EPF-Lausanne where one side-wall of a Laval nozzle has been replaced by a mirror surface.

The mirrored surface supports the fixation of the test model and allows the tunnel wall to be instrumented. However due to the rigid body movement of the facility spurious vibration information is added to the interferometrically measured transonic flow data.

To separate the vibration data from the flow data a numerical method has been developed by Warwick University. The method uses a Digital Fast Fourier Transform (DFFT) algorithm to remove the superimposed background information and then extracts quantitative numerical data automatically by the use of a method defined as phase unwrapping. The method is described in greater detail by Judge in ref. (4).

An example of a transonic flow around a DCA-Profile (cord length = 75.7 mm) is demonstrated on the Laval nozzle flow facility at EPF-Lausanne.

2 EXPERIMENTAL SET-UP AND DESCRIPTION

2.1 The supply of compressed air

The radial compressor of the "Laboratoire de Thermique Appliquée et de Turbomachines" (LTT) is driven by an electric engine of 2500 kW at constant rotational speed. The pressure at the outlet of the compressor is regulated with a valve at the inlet. The maximum pressure ratio is 4 and the maximum mass flow is 10 kg/s. The compressed air passes through a heat exchanger where the temperature can be adapted to the need of the test rig. The maximum value is the compressor outlet temperature (170 – 200 °C) the minimum temperature is 15 °C.

After having passed through the heat exchanger the air enters the settling chamber and then the Laval nozzle.

2.2 The Laval nozzle

In the settling chamber (1) (see Fig. 1) the total pressure and total temperature is measured. The upper and the lower liners (2) are flexible; it is therefore possible to regulate continuously the outlet flow velocity between $0.05 \leq M \leq 1.6$.

For the present measurements these liners are regulated convergent with a final distance of 180 mm at the end.

In the centerline of the side walls two horizontal rows of respectively 5 pressure taps (11-15; 21-25) are situated to control the flow development and two vertical rows (16-20; 26-30) to control the flow symmetry.

The DCA-profile (6) with a cord length of 75.5 mm and a thickness of 4 mm is fixed in the steel mirror (4) and in the Plexiglas window (5). The steel mirror contains also 6 pressure taps (6-10; 28).

On the profile at mid-span there are 4 pressure taps on the upper and lower surface. Their chord wise position is given in Figure 1. The measured pressure values are given in Appendix A1.

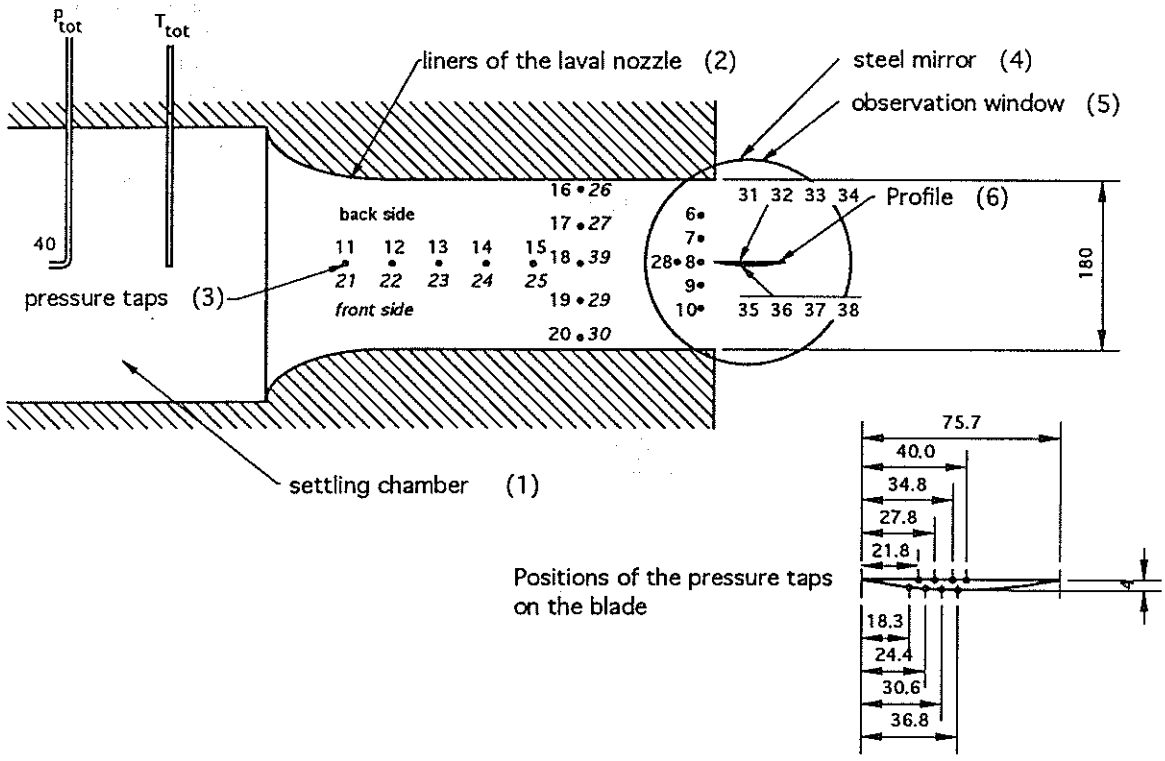

Fig. 1: Experimental set-up in the Laval nozzle

2.3 The reflecting holographic system

Figure 2 shows the principle set-up of the reflecting holographic system. The Ruby Pulse Laser (1) has the following characteristic:

WAVELENGTH	694 nanometers
OUTPUT ENERGY	1 J total
MAX. REP RATE	4 Pulses / min.
COHERENCE LENGTH	Greater than 1m
PULSE DURATION	30 ns nominal
POLARISATION	Vertical

The focused laser beam was divided using a beamsplitter (2) into an object and reference beam. The object beam has been expanded and collimated by the combination of a lens (3), diaphragm (4), plane mirror (6) and concave mirror (5); to pass through the flow region perpendicular to the main flow direction.

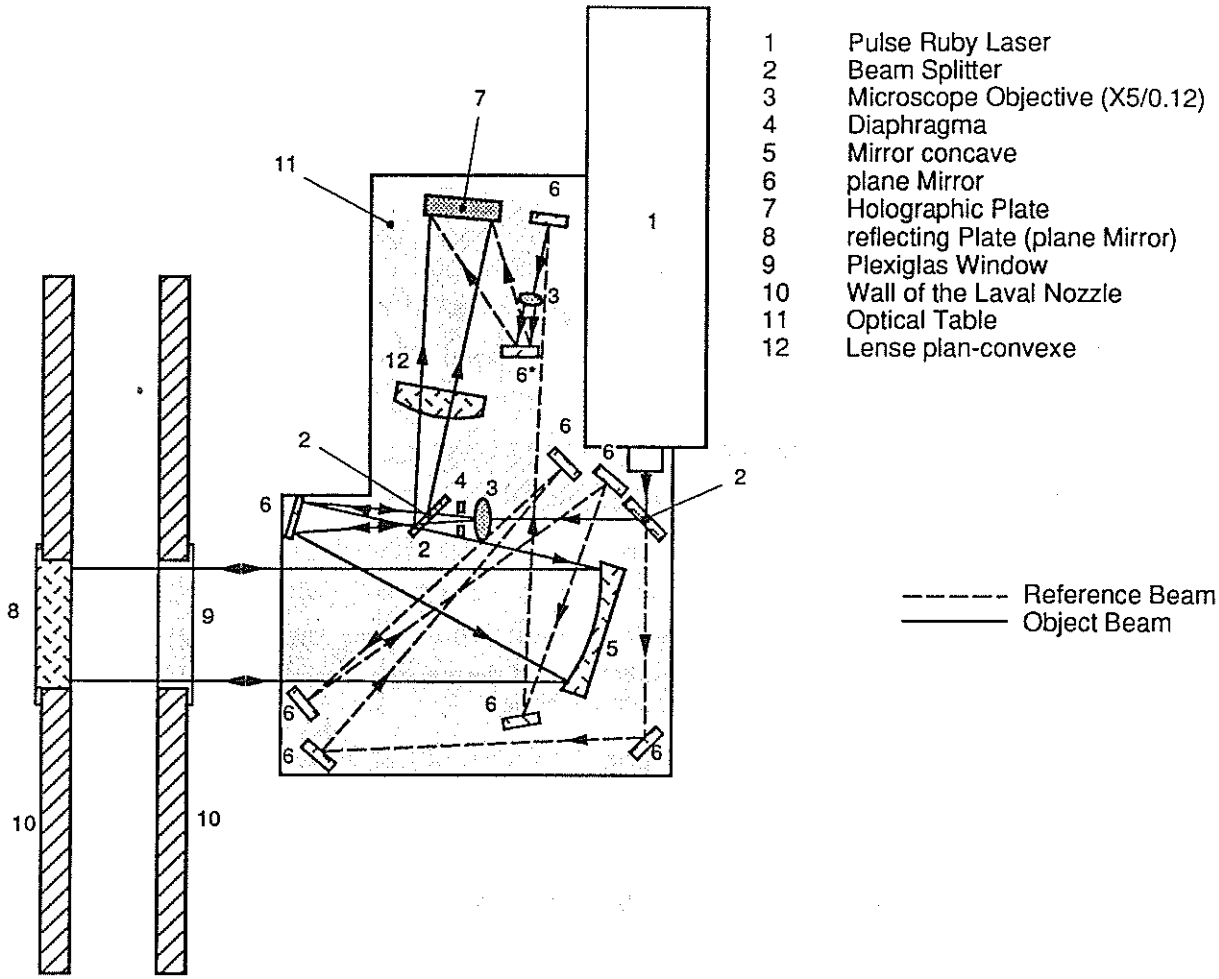

Fig. 2: Set-up of the reflecting system

The object beam is then reflected back along the same optical path, turned by a second beamsplitter (2), passed through a second lens (12), and is imaged onto the holographic film plate (7).

The reference beam, which encodes the interferometric data onto the holographic plate, has been reflected by several mirrors (6), to achieve a path length match with the sample beam, then expanded (3), to be recombined with the object beam on the holographic film plate (7).

The method of taking the hologram was performed as following:

- Making a first exposure with a transonic flow present,
- Tilting slightly the reference beam by making a lateral rotation of mirror 6* (fig. 2),
- Making a second exposure without the flow.

2.4 The reconstruction set-up

Figure 3 shows the set-up for reconstructing the hologram. A slide projector (1) is used as a source of white light. The lens (3) collimates the light beam to reconstruct the holographic plate. The reconstructed wave-front of the object beam is then projected into the film plane of a camera to create a photographic image.

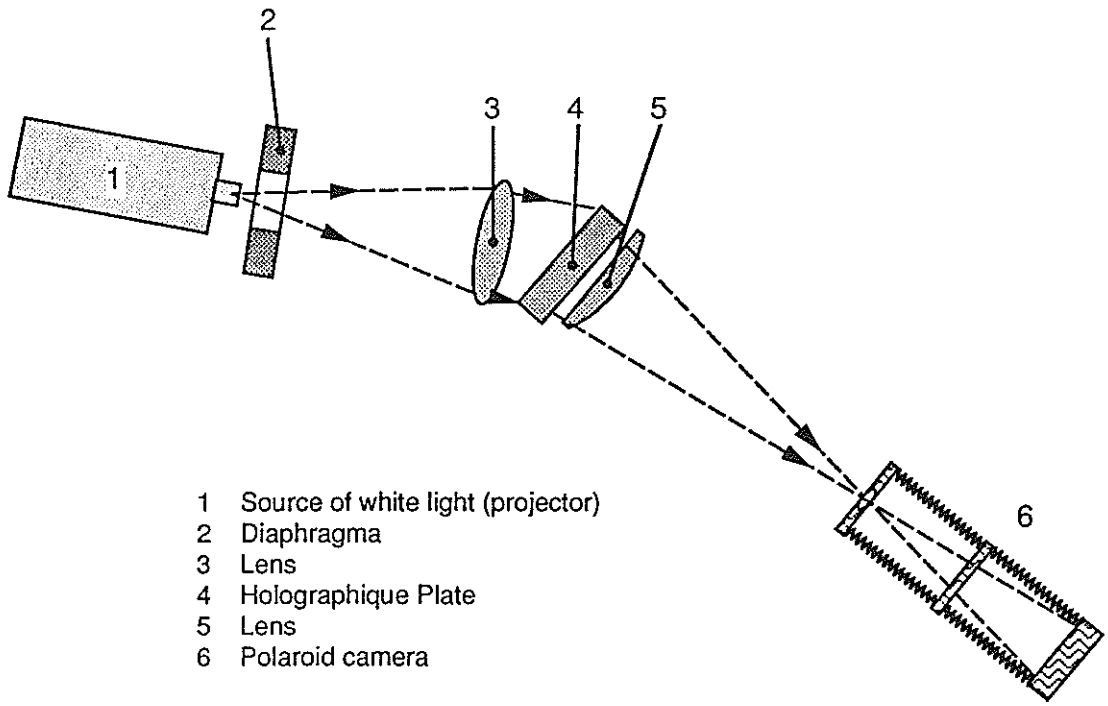

Fig. 3 *Set-up of the reconstruction system*

3 FRAN IMAGE PROCESSING AND SOFTWARE DEVELOPMENT

3.1 Fourier transform fringe analysis

The Fourier transform method of fringe-pattern analysis is a powerful way of evaluating conventional interferograms. A high spatial carrier frequency is introduced by tilting the wave-front. In the case of the example presented this has

been achieved by moving the position of the reference beam between holographic exposures.

As a result of this movement, the reconstructed image has a spatial carrier fringe pattern in addition to the phase information encoded by the change in refractive index. The phase function must be a slowly varying function compared to the variation introduced by the carrier frequency.

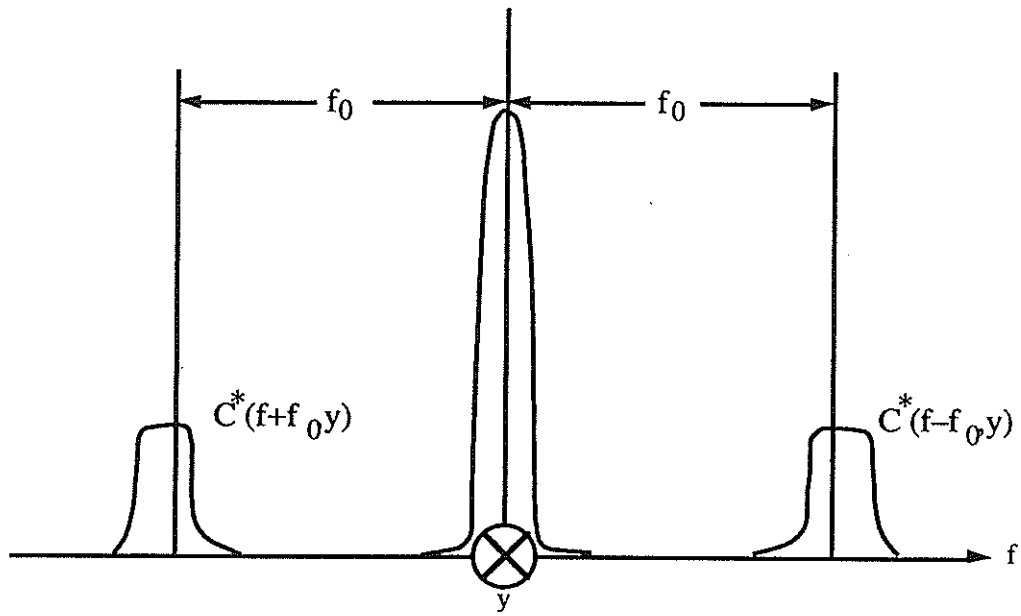

Fig. 4a *Separated Spectra of Fringe Pattern*

The FFT spectra can be separated into the carrier frequency, as shown in Fig. (4a) and a low frequency intensity modulation component. Only one of the two spectral sidelobes is necessary to calculate phase. The selected lobe is translated to the origin, as is shown in Fig. (4b). Next, by applying the inverse Fourier transform a phase map is obtained.

The wrapped map has two pieces of information which have been used to create a contiguous map. Firstly from the inverse Fourier transform by dividing the real by the imaginary component a Tangent function, or Tan wrapped map has been created. This function is discontinuous and defines the direction of the fringe gradient. Secondly the images can now be phase unwrapped automatically using a computer algorithm which circumvents both spike noise and local area inconsistencies.

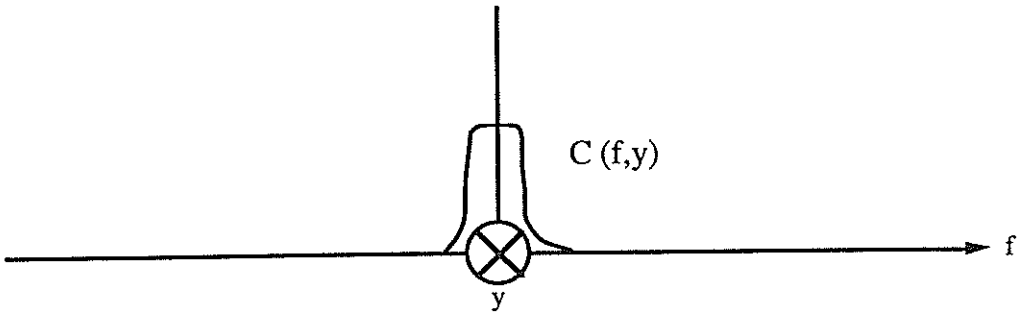

Fig. 4b *One of the Side Lobes Translated to the Origin*

3.2 The minimum spanning tree approach to phase unwrapping, applied to the FFT method.

The minimum spanning tree is a mechanism for computing the consistency of possible phase unwrapping routes. Effectively the images are divided in small 'tiles' of approximately 30 x 30 pixels each. The quality of fringe information within each tile is assessed. If the tile has a high noise level, detected as a rapid variation in the pixel value it is given a low weighting. If the quality is high it is given a high weighting. The high weighting value tiles are then joined on a hierarchical basis using a minimum spanning tree strategy.

The tree uses a hierarchical unwrapping strategy at the lowest level paths between pixels are compared to circumvent spike noise. At the higher level tiles of pixels are compared to circumvent aliasing induced inconsistencies and natural inconsistencies. The minimum spanning tree approach therefore presents a noise immune phase unwrapping strategy.

3.3 Application of FRAN to the EPFL Image.

The image provided by EPFL has presented two main problems to the software. In the first case the photograph was printed and then digitised using a standard document scanner to a resolution of 2,000 x 3,000 pixels. At this resolution the individual tiles at 30 x 30 pixels were small enough in size, to find a path through both the wake and shock regions of the image.

The second aspect of the problem was more difficult to solve. The effect of the linear rigid body movement of the test section added extra fringes to the interferometric

data. In the FFT approach the carrier frequency is removed by applying a frequency shift in Fourier space. It was not possible to determine exactly what this frequency should be, so in the case of figure (6), it has been determined by frequency shifting the information and by matching the measured fringe value at several points in the image with static pressure measurements.

4 RESULTS

4.1 Flow conditions

The experiment was performed with the following flow conditions:

Angle of the profile:	$\alpha = 0°$
Number of Mach:	$M = 0.79$
Total pressure:	$p_\infty = 1376.6$ mbar
Total temperature:	$T_\infty = 22.8$ °C
Ratio of specific heats:	$\kappa = 1.4$

The Mach number was calculated using equation (4.1) where p is the static pressure at position 39 (see Figure 2)

$$M = \sqrt{\frac{2}{\kappa - 1} \cdot \left[\left(\frac{p_\infty}{p} \right)^{\frac{k}{k-1}} - 1 \right]} \qquad (4.1)$$

4.2 The holographic images

Figure 5 shows a Polaroid photograph image made using the reconstruction set-up described in (Fig. 3).

It can be seen that the optical quality is not optimal. There are scratches in the observation window and the lower part of the image is to dark to process. However the processed image (Fig. 6) is relatively clear. It is a very good illustration of the effectiveness of this type of automatic processing.

There are some regions where the process could not solve the image. Near the leading edge there are not sufficient carrier fringes, thus closed fringe circles are formed. Near the blade surface there are also an unsolved region caused by reflected images of the blade fixture system.

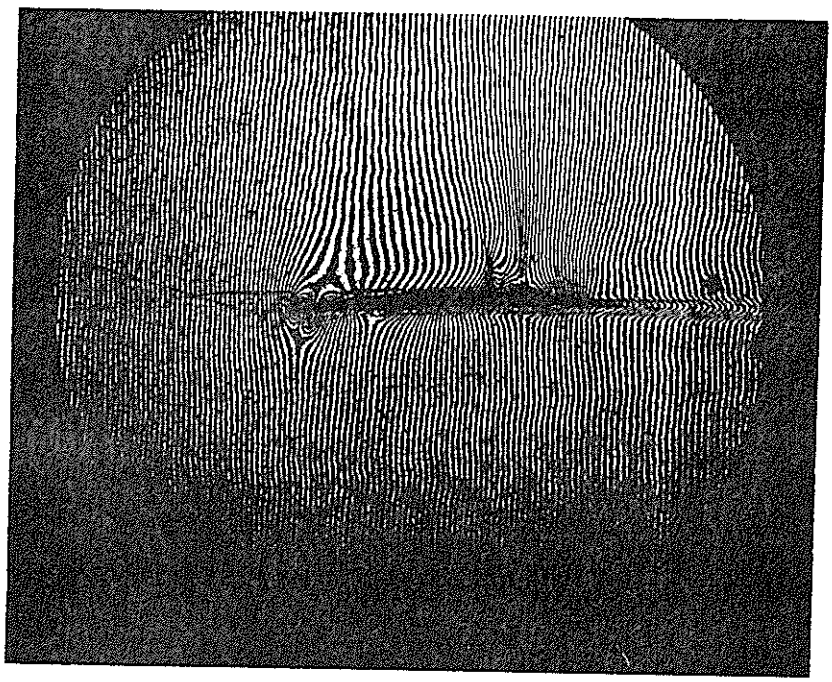

Fig. 5 *The Polaroid image*

However the software has successfully made a contiguous density map of the flow. The rapid fringe changes associated with the wake and shock regions have been visualised in a quantitative manner.

In Figure 7 a contiguous three-dimensional view of the density map of the transonic flow has been plotted is seen. It is possible to observe a deceleration towards the leading edge, an acceleration on the suction side with a weak shock and a nearly constant flow velocity on the pressure side. Also, the lower velocities in the wake can clearly be seen.

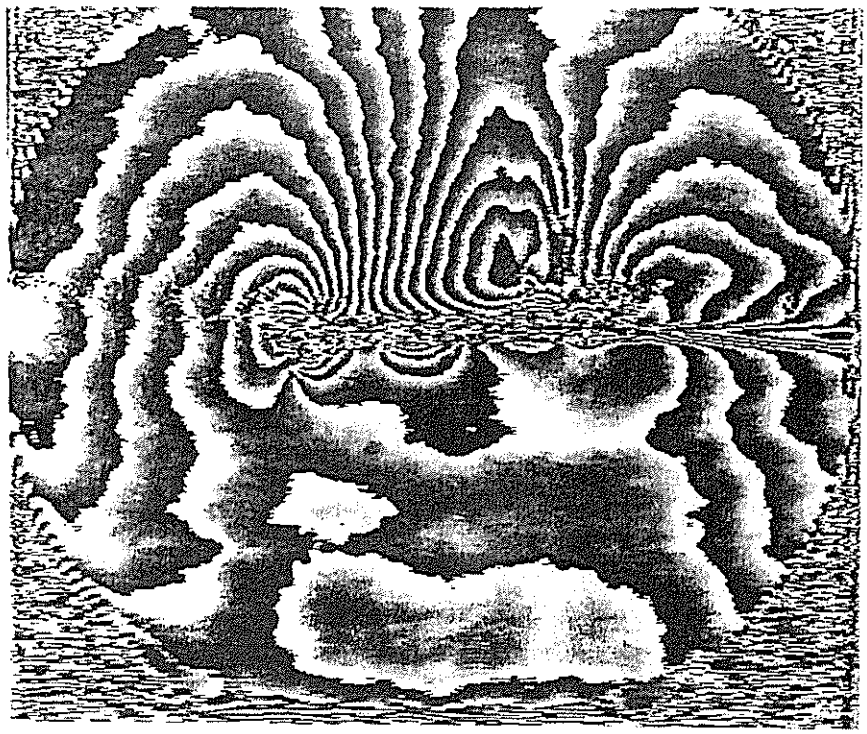

Fig. 6 *The solved fringe image*

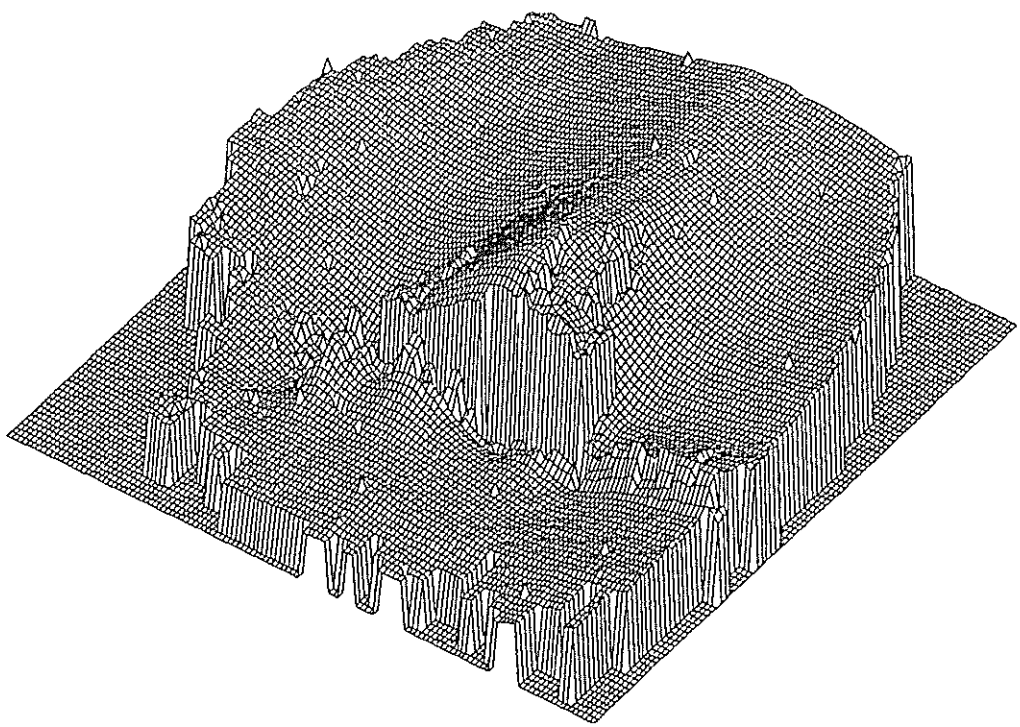

Fig. 7 *Three dimensional view*

5 CONCLUSIONS

A quantitative whole field visualisation of the transonic flow around a 2D blade profile has been demonstrated using LHI.

The LHI test system was restricted in optical access to one side of the test facility, allowing a conventional instrumentation and blade fixing methods to be used.

Superimposed vibrations from the Laval nozzle have been removed by the use of a digital Fast Fourier Transform algorithm and numerical data has been extracted by a technique known as phase unwrapping.

The success of this method has demonstrated that a wide range of flow applications could now be investigated in a non-intrusive quantitative manner using optical diagnostics.

REFERENCES

1. Bryanston-Cross P.J., Lang T., Oldfield M. and Norton R., *"Interferometric Measurements in a Turbine Cascade using Image Plane Holography", Journal of Engineering for Power, January 198l.*

2. P.J. Bryanston-Cross, "High Speed Flow Visualisation". *Prod. Aerospace Science, Vol. 23, pp. 85-l04, l986.*

3. S.Parker, C.M.Holden & P.J.Bryanston-Cross., "Quantitative *3 D Holographic Interferometry." Presented at the IMechE conference on Optical Methods and data processing in heat and fluid flow. 2-3 April 1992.*

4. Judge T.J. "The application of digital imaging to fringe analysis and PIV (particle image velocimetry)." Phd thesis presented April 1992, Department of Engineering, Warwick University.

ANNEX

Appendix A1: *Measured pressures in [mbar] (see fig. 2)*

```
TITTLE MW 3.4.1992 refl.DCA alpha=0
26-2 T=22.8
    5    956.0    6    905.3    7    912.0    8    928.8
    9    913.4   10    897.2   11    983.9   12    930.7
   13    923.6   14    917.6   15   1021.6   16    896.2
   17    895.4   18    901.9   19    898.0   20    896.6
   21    976.8   22    929.5   23    922.9   24    917.6
   25    911.9   26    901.8   27    895.7   28    912.3
   29    894.3   30    892.8   31    895.8   32    907.9
   33    901.1   34    905.5   35    785.5   36    735.7
   37    693.9   38    656.2   39    901.8   40   1376.6
```